Journal of Catalysis **198,** 77–88 (2001)
doi:10.1006/jcat.2000.3082, available online at http://www.idealibrary.com on IDEAL®

Impact of Calcination Conditions on the Structure of Alumina-Supported Nickel Particles

Bron Vos, Eduard Poels, and Alfred Bliek[1]

Department of Chemical Engineering, University of Amsterdam, Nieuwe Achtergracht 166, 1018 WV Amsterdam, The Netherlands

Received July 20, 2000; revised September 24, 2000; accepted September 28, 2000; published online February 1, 2001

Alumina-supported nickel catalysts are widely used in industry. The synthesis of these catalysts often proceeds through coprecipitation: following the precipitation of nickel salts and drying, the material is calcined, reduced, and passivated. Each of these steps may influence the catalyst ultimately obtained. In the present study, the synthesis conditions were systematically investigated. Following precipitation, a hydrotalcite is formed. Starting from hydrotalcite precursors with varying Ni/Al ratios, the conversion to the ultimate Ni-on-alumina catalyst was studied, using TEM, TPR, XRD, and chemisorption. In particular, we examined the effect of water vapour and acidic gases—liberated during calcination—on the morphology of the catalyst ultimately obtained. Two competing mechanisms for the formation of the ultimate catalyst morphology are suggested.

Key Words: **Ni/Al_2O_3; morphology; calcining; coprecipitation; hydrotalcite.**

1. INTRODUCTION

Supported nickel catalysts are widely used in industry in, for example, the production of synthesis gas, steam reforming, fat hardening, hydrogenation of aromatics, and isomerisation of hydrocarbons (1). These catalysts are conventionally prepared by impregnation, deposition precipitation, or coprecipitation. Subsequently, the material is dried, calcined, reduced, and passivated. The conditions during each of these steps influence the properties and morphology of the material ultimately formed.

The preparation of alumina-supported nickel using coprecipitation has been investigated by several groups (2–27). On coprecipitation of an aqueous solution of soluble nickel and aluminum salts, rather than the formation of the separate hydroxides, a compound is formed with a layered structure (2, 3). The precipitate is a mineral of the hydrotalcite group (4–6, 28). The stability of the hydrotalcite depends on the Ni/Al ratio (7). Stable hydrotalcite-like materials are formed for a Ni to (Ni + Al) molar ratio between 0.5 and 0.85 (6, 8). When nickel and aluminum nitrate are used, a lower pH of precipitation generally leads to an increasing amount of nitrates present in the hydrotalcite (6, 9). Although the nickel crystallite size of the ultimate material hardly depends on the pH of precipitation, the morphology of the material is influenced by the pH (10). The temperature of the liquid during precipitation and the period of time involved in the precipitation are less important (9, 11).

During calcination of the hydrotalcite, the material decomposes. The decomposition products vary with calcination temperature (5, 8, 9, 11–13, 29, 30). At low temperature (330°C), the components interact and two mixed oxides are formed: one NiO-rich phase containing some aluminum ions and an Al_2O_3-rich phase containing nickel ions. It has been suggested that the presence of sodium promotes the formation of aluminates (9). The size of the NiO particles increases with temperature and Ni/Al ratio (7–9, 14, 15, 24). The NiO-rich particles can be viewed as decorated by nickel aluminate phases (16, 17). The NiO particles may also be visualised as supported by a nickel aluminate phase (14). A higher Ni/Al ratio promotes the formation of NiO (25, 27).

At high temperatures (>730°C), nickel oxide and a nickel aluminate spinel are formed. The presence of aluminum ions in or near the NiO particles may act to stabilise the NiO particles against sintering (8, 14, 15). However, the presence of nickel aluminate spinel phases renders the reduction of the nickel oxide phase more difficult (15, 18–21, 26).

It has been observed that a higher hydrogen space velocity during reduction results in an increased degree of reduction (8, 31). Reduction of the NiO crystallites is inhibited by water, probably as adsorbed water hinders hydrogen adsorption/dissociation and nucleation of Ni^0 atoms (22, 32–35). Nickel aluminate is still present in the material after reduction (20, 21). The presence of sodium aluminate accelerates the growth of the nickel crystallites (9, 23). It has been demonstrated that porous nickel aluminate shells decorate the metallic nickel (17). The nickel aluminate phase is reduced at temperatures in excess of 800°C (36, 37). However, the nickel crystallites tend to grow and the degree of reduction increases as the reduction temperature or Ni/Al

[1] To whom correspondence should be addressed. Fax: 31-20-525-5604. E-mail: Bliek@its.chem.uva.nl.

0021-9517/01 $35.00

ratio is raised (7, 8, 24, 27). It has been suggested that sintering of the metallic nickel crystallites upon reduction is hindered by the presence of smaller adjacent alumina crystallites (8, 21, 38). The presence of the alumina crystallites prohibits direct physical contact between adjacent nickel particles. Consequently, a direct relation exists between the particle size of the nickel oxide rich phases of the calcined materials and those of the reduced materials.

As mentioned before, each step of the synthesis procedure may influence the catalyst ultimately obtained. In order to produce tailor-made catalysts it is therefore necessary to know in what way the structure of the material changes during each subsequent synthesis step. Doesburg *et al.* studied the morphology of coprecipitated Ni/Al_2O_3 using SEM (10). It was found that the morphology after each preparation step (coprecipitation, calcination, reduction, and passivation) hardly changes: the material resembles a spongelike structure, consisting of rod-shaped particles. TEM imaging showed that the material after coprecipitation has a platelike structure and after calcination at 650°C some particles, probably NiO, appear (14).

In the present work, the preparation of Ni/Al_2O_3 samples from a hydrotalcite precursor is studied. The textural properties of the materials obtained after each synthesis step were analysed using TEM, TPR, XRD, and chemisorption. It has been suggested that a relation exists between the structure of the material obtained after calcination and the structure of the reduced material. We will focus on the impact of calcination conditions on the morphology of the final material after reduction and passivation. Materials with different Ni/Al ratios were investigated.

2. MATERIALS AND METHODS

2.1. Synthesis

2.1.1. Precursor Materials

Several Ni/Al_2O_3 samples with different nickel loadings were prepared by coprecipitation (6, 8). To this end, an aqueous solution of nickel nitrate (Merck, ≥99%) and aluminum nitrate (Koch, p.a.), with a total nickel and aluminum concentration of 1.8 $mol \cdot dm^{-3}$, was used. A stoichiometric amount of precipitating agent, a sodium hydroxide (Merck, ≥99%) solution (5 $mol \cdot dm^{-3}$), was used. Over a period of 1 h, 350 cm^3 of the nitrate solution and 350 cm^3 of the sodium hydroxide solution were added simultaneously to a double-walled vessel (volume 1.5 dm^3) containing 300 cm^3 of distilled water. The solutions were injected below the surface of the solution in the vessel using Gilson Minipuls 2 dosing devices. The admixing of the solutions was controlled in such a way as to maintain the pH at 8 ± 0.2 (Inlab 412/170 pH electrode). The content of the vessel was vigorously stirred (Heidolph Type RZR1 stirrer motor; 2000 rpm) and kept at a temperature of 80°C by recirculating the water of a water bath between the walls of the vessel. A green precipitate was formed, which was aged in the mother liquor overnight at 80°C, removed, and washed thoroughly with distilled water until the pH of the supernatant liquid was 7. The green precipitate was dried in an oven at 120°C overnight.

2.1.2. Calcination

2.1.2.1. Procedure 1. After the green precipitate was dried, it was calcined in a fixed bed reactor in a flow of air (SV (space velocity) $= 4 \times 10^{-4}\ m^3 \cdot s^{-1} \cdot kg^{-1}$) at 450°C for 10 h (samples A01 and B01, depending on nickel loading; see Table 3). The temperature was first raised to 200°C at a heating rate of 1°C per minute and maintained there for an hour. It was further raised to 450°C at a heating rate of 0.5°C per minute.

2.1.2.2. Procedure 2. The green precipitate was calcined in a fixed bed reactor under stagnant conditions at 550°C for 10 h with a heating rate of 5°C per minute (samples A02 and B02).

2.1.2.3. Procedure 3. The dried green precipitate was calcined in a fixed bed reactor in a flow of air ($SV = 2 \times 10^{-4}\ m^3 \cdot s^{-1} \cdot kg^{-1}$) at 430°C for 10 h. The temperature was first raised to 200°C at a heating rate of 1°C per minute and maintained there for an hour. It was subsequently raised at a rate of 0.5°C per minute.

All samples were heated in moist air ($SV = 2 \times 10^{-3}\ m^3 \cdot s^{-1} \cdot kg^{-1}$), obtained by saturating air at ambient temperature with water. The resulting water concentration was 2.4 vol%. Various samples were prepared using different final temperatures and using different dwell times (see Table 1). The heating rate was 5°C per minute for all samples.

2.1.3. Reduction and Passivation

After cooling to room temperature, calcined samples were reduced in a H_2/Ar flow (gas-phase composition, 2/1 v/v) at 550°C for a period of 24 h (sample series A and B) or 2 h (sample series C and D), respectively. The

TABLE 1

Final Temperature and Dwell Time during Treatment in Moist Air

Sample	Final temperature (°C)	Dwell time (h)
C1, D1	450	1
C2, D2	500	1
C3, D3	550	1
C4, D4	550	4

Note. Sample series C has a lower nickel loading than sample series D.

TABLE 2

Space Velocities Used during Reduction and Passivation

Sample series	SV ($m^3 \cdot s^{-1} \cdot kg^{-1}$)	
	Reduction	Passivation
A, B	2×10^{-4}	2×10^{-4}
C, D	6×10^{-4}	1×10^{-3}

reduction temperature was first raised to 150°C at a heating rate of 1°C per minute and maintained there for an hour. It was further raised to 550°C at a heating rate of 0.5°C per minute. After reduction, the sample was allowed to cool to room temperature in Ar and passivated in a stream of O_2/Ar (0.5 vol% O_2). The different space velocities used during reduction and passivation are shown in Table 2.

2.2. Characterisation

2.2.1. H_2 Chemisorption and O_2 Uptake

Hydrogen chemisorption and oxygen uptake studies on Ni/Al_2O_3 samples were carried out using a Sorptomatic 1900 (Carlo Erba). About 1 g of the passivated material was reduced in a H_2/He flow (2/1 v/v, SV = 2×10^{-3} $m^3 \cdot s^{-1} \cdot kg^{-1}$) at 400°C for 2 h. The reduction temperature was first raised to 150°C at a heating rate of 5°C per minute and maintained there for an hour. It was further raised to 400°C at a heating rate of 1°C per minute. After reduction, the temperature was kept at 400°C in a He flow (SV = 2×10^{-3} $m^3 \cdot s^{-1} \cdot kg^{-1}$) for 1 h and thereafter allowed to cool to room temperature under a He flow. The sample was transferred to the Sorptomatic under a He atmosphere. After evacuation to 10^{-6} mbar, hydrogen adsorption and desorption isotherms at 25°C were measured. Following chemisorption, the same material was heated to 400°C and degassed for 1 h to give a pressure of 10^{-6} mbar. Oxygen uptake was measured at 400°C.

The nickel metal size was calculated after extrapolation to zero pressure, assuming a surface area of 6.77 nm^2 per nickel atom and spherical metal particles (39). The degree of reduction was determined by the above-described reaction with oxygen.

2.2.2. Transmission Electron Microscopy

Transmission electron microscopy (TEM) was performed using a Philips CM 30 T electron microscope with a LaB_6 filament as the source of electrons operated at 300 kV. Samples were mounted on a microgrid carbon polymer supported on a copper grid by placing a few droplets of a suspension of ground passivated sample in ethanol on the grid, followed by drying at ambient conditions. Qualitative elemental analysis was performed using a LINK EDX system.

2.2.3. Elemental Analysis

The nickel content was quantitatively established by inductively coupled plasma atomic emission spectroscopy (ICP-AES) using a multichannel Thermo Jarrel Ash ICAP 957 spectrometer, upgraded to Model ICAP 61. Prior to analysis, aqua regia extractions of the material were made. The mean value of four replicate measurements was used; the standard deviation of these measurements was about 1%.

2.2.4. Temperature-Programmed Reduction

A conventional TPR setup was used. The sample under study was placed in a quartz tubular reactor. The sample bed contained approximately 25 mg of sample, weighed to 0.1-mg accuracy. A H_2/Ar mixture (2/1 v/v) was used (SV = 1×10^{-2} $m^3 \cdot s^{-1} \cdot kg^{-1}$). The heating rate employed was 5 $K \cdot min^{-1}$.

2.2.5. X-Ray Diffraction

X-ray diffraction (XRD) analysis of passivated Ni/Al_2O_3 samples with varying nickel loading was performed on a Philips PW 1830 diffractometer using CuKα (λ = 0.154056 nm) radiation.

3. RESULTS

The microstructure of Ni/Al_2O_3 samples after precipitation, calcination, reduction, and passivation was studied using TPR, XRD, and electron microscopy. The changes of the structure due to each subsequent step were analysed.

Nickel and aluminum content of the passivated Ni/Al_2O_3 samples was determined by elemental analysis. An overview of all the samples used in this study is given in Table 3.

Sample series A and B are used to discuss the effect of calcining under flow or stagnant conditions on the ultimate properties of the material. Series C and D are introduced to study the combination of prolonged treatment in stagnant moist air and high temperature during calcination.

3.1. Calcining under Flow or Stagnant Conditions

3.1.1. Precursor Materials

After precipitation, washing, and drying, precursor materials for sample series A and B were obtained.

The precursor materials for both the 37 wt% Ni/Al_2O_3 sample (sample A00) and the 56 wt% Ni/Al_2O_3 sample (sample B00) consist of platelike structures. The average size of the structures is larger for sample A00 than for sample B00, as shown in Fig. 1. EDX analysis of the area shown in the images indicated that the material consists of aluminum and nickel. The platelike structures observable in TEM probably are brucite-type hydroxide layers with the

TABLE 3

Ni/Al_2O_3 Samples Used in This Study

Sample	Ni content (wt%)	State of the material: Calcination procedure	Reduced	Passivated	x_{Ni} (= Ni/(Ni + Al) (mol/mol)
A00	37	—	—	—	—
A01	37	1	—	—	—
A02	37	2	—	—	—
A11	37	1	+	+	0.4
A12	37	2	+	+	0.4
B00	56	—	—	—	—
B01	56	1	—	—	—
B02	56	2	—	—	—
B11	56	1	+	+	0.6
B12	56	2	+	+	0.6
C1	33	3	+	+	0.4
C2	33	3	+	+	0.4
C3	33	3	+	+	0.4
C4	33	3	+	+	0.4
D1	54	3	+	+	0.7
D2	54	3	+	+	0.7
D3	54	3	+	+	0.7
D4	54	3	+	+	0.7

composition $[Ni_xAl_{1-x}(OH)_2]^{(1-x)+}$ (6). The excess charge of the layers is compensated by the incorporation of anions, such as NO_3^- and OH^-, in the spaces between the layers (interlayers). Molecular water is also included in the interlayer.

The presence of a hydrotalcite structure in the green samples is confirmed by XRD analysis (Fig. 2).

In addition to the hydrotalcite phase, a boehmite aluminum hydroxide phase is observed in sample A00 (5, 14, 30, 40). A single-phase layer structure only exists for $x_{Ni} \geq 0.50$; below this limit, Kruissink *et al.* observed the presence of boehmite using X-ray diffraction (6). It is not possible to discriminate between pure nickel hydroxide and the hydrotalcite because reflections of these phases overlap. EDX analysis of our samples during TEM, however, shows that nickel and aluminum are found throughout the platelike structures. No discrete nickel hydroxide or aluminum hydroxide phases could be detected. The boehmite phase present in sample A00 therefore probably contains some nickel.

3.1.2. Samples after Calcination

TEM analysis (Fig. 3) shows that sample A01 contains more crystalline material than the other calcined materials (samples A02, B01, and B02). Nickel-containing particles and some alumina are also observed.

Most likely three phases have been formed: a nickel oxide phase, a nickel-containing aluminum oxide phase, and a nickel aluminate spinel phase (14). Less platelike material is present after calcination procedure 2 (under stagnant conditions; samples A02 and B02) than after calcination procedure 1 (in a flow of air; samples A01 and B01). The alumina phase becomes amorphous during calcination procedure 1.

The dark particles that are visible on the alumina support clearly contain much more nickel according to EDX elemental analysis than the surrounding support material.

For both sample A01 and sample B01, the average particle size of the nickel-containing particles after calcination procedure 1 is smaller than the nickel particle size in the materials after calcination procedure 2 (samples A02 and B02).

From XRD patterns (Fig. 4) it is difficult to discriminate between $NiAl_2O_4$ and Al_2O_3 because reflections of these phases overlap. Both phases are X-ray amorphous, as evidenced by broad reflections. After calcination procedure 2, the bands that represent the nickel oxide phase become

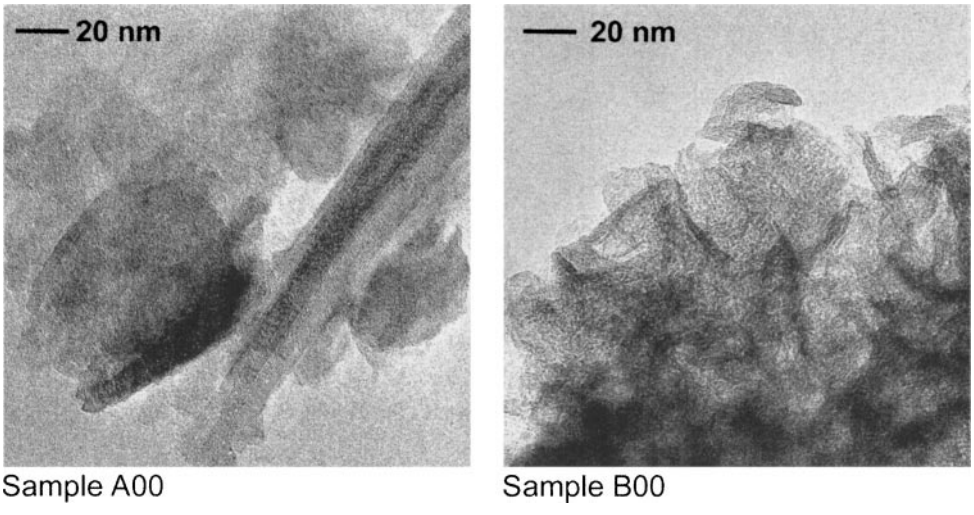

FIG. 1. TEM images of (green) precursor materials of 37 wt% Ni/Al_2O_3 (A00) and 56 wt% Ni/Al_2O_3 (B00). Dark areas represent nickel phase.

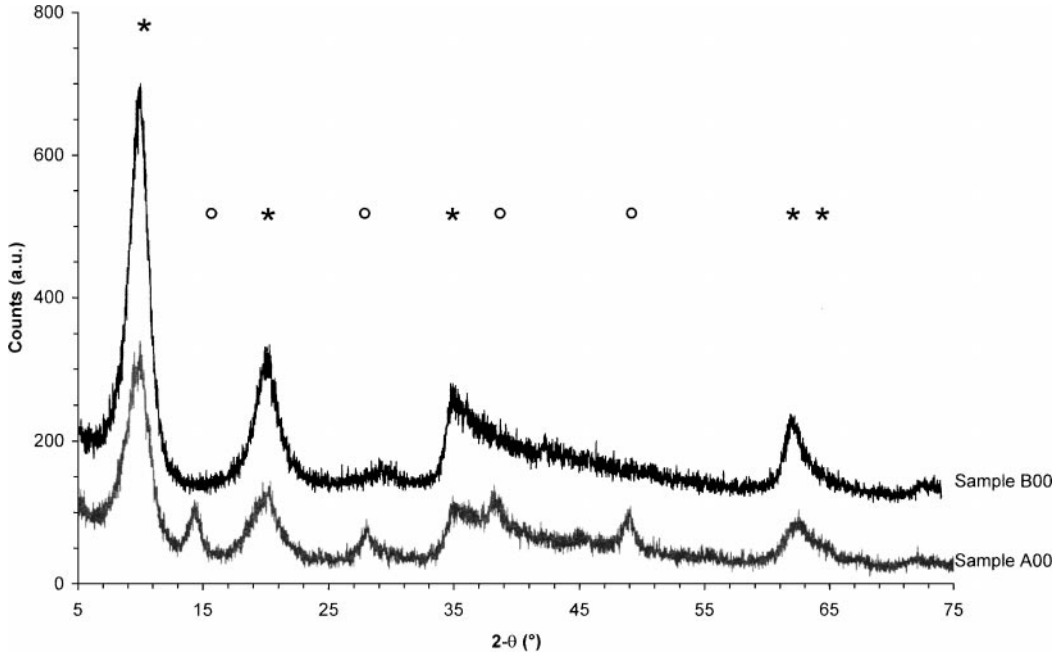

FIG. 2. XRD patterns of the precursor materials: (○) reflections of boehmite-like aluminum hydroxide phase; (∗) reflections of hydrotalcite-type structure.

narrower, indicating that calcination procedure 2 results in larger nickel oxide particles.

Three bands can be distinguished in TPR of the calcined Ni/Al_2O_3 samples (Fig. 5) (20, 21, 32, 41). A first reduction band is observable between 250 and 350°C. The reduction of nickel oxide in sample A02 and sample B02 takes place at lower temperature than in sample A01 and sample B01. Interaction between nickel oxide and alumina tends to increase the reduction temperature of the nickel oxide. Comparing sample A01 with A02 and B02 with B01, it is apparent that fewer aluminum ions are present in the nickel oxide phase after calcination under stagnant conditions (A02 and B02), resulting in a lower reduction temperature of the nickel oxide. From 350 to 600°C, the reduction of nickel oxide containing aluminum is observed; at higher temperatures, reduction of nickel contained in the alumina phase is seen.

3.1.3. Samples after Reduction and Passivation

Both passivated sample A11 and sample A12 (Fig. 6) contain less crystalline material than the materials after calcination procedure 1 only (samples A01 and A02). After calcination procedure 2 (calcination under stagnant conditions), the crystalline material is probably less stable toward reduction. More nickel-containing particles are present than in samples A01 and A02.

In the TPR patterns of the passivated Ni/Al_2O_3 samples (Fig. 7), two reduction bands can be distinguished (20, 21, 32, 41). Around 200°C the reduction of the passivation layer of oxygen can be seen. The presence of nickel aluminate in the samples is evident from the observed reduction band between 600 and 800°C. Samples calcined using procedure 1 contain less nickel aluminate than samples calcined using procedure 2.

Reflections of $NiAl_2O_4$ and Al_2O_3 in the XRD patterns (Fig. 8) overlap. The $NiAl_2O_4$ phase and Al_2O_3 phase are amorphous; the nickel metal phase is more crystalline.

The average particle size of the nickel-containing particles in sample B11 determined by hydrogen chemisorption is smaller than in sample B12 (Fig. 9).

Samples A11 and A12 have the same degree of reduction, but the nickel particles of sample A12 are slightly larger. Sample B12 has a lower degree of reduction than sample B11, but the nickel particles of sample B12 are larger. Obviously, higher metal loading in B samples results in larger nickel crystallites (Fig. 9).

3.2. Treatment of Calcined Catalyst in Moist Air at High Temperature

Catalysts that are calcined and subsequently treated in moist air at temperatures exceeding those during calcination exhibit reducibility changes (Fig. 10).

The degree of reduction in sample series C ($x_{Ni} = 0.4$) in hydrogen increases with treatment temperature. After treatment at high temperature for a prolonged period of time, the reducibility decreases. On the other hand, sample series D ($x_{Ni} = 0.7$) shows a steady decrease in the degree of reduction with increasing pretreatment temperature and time.

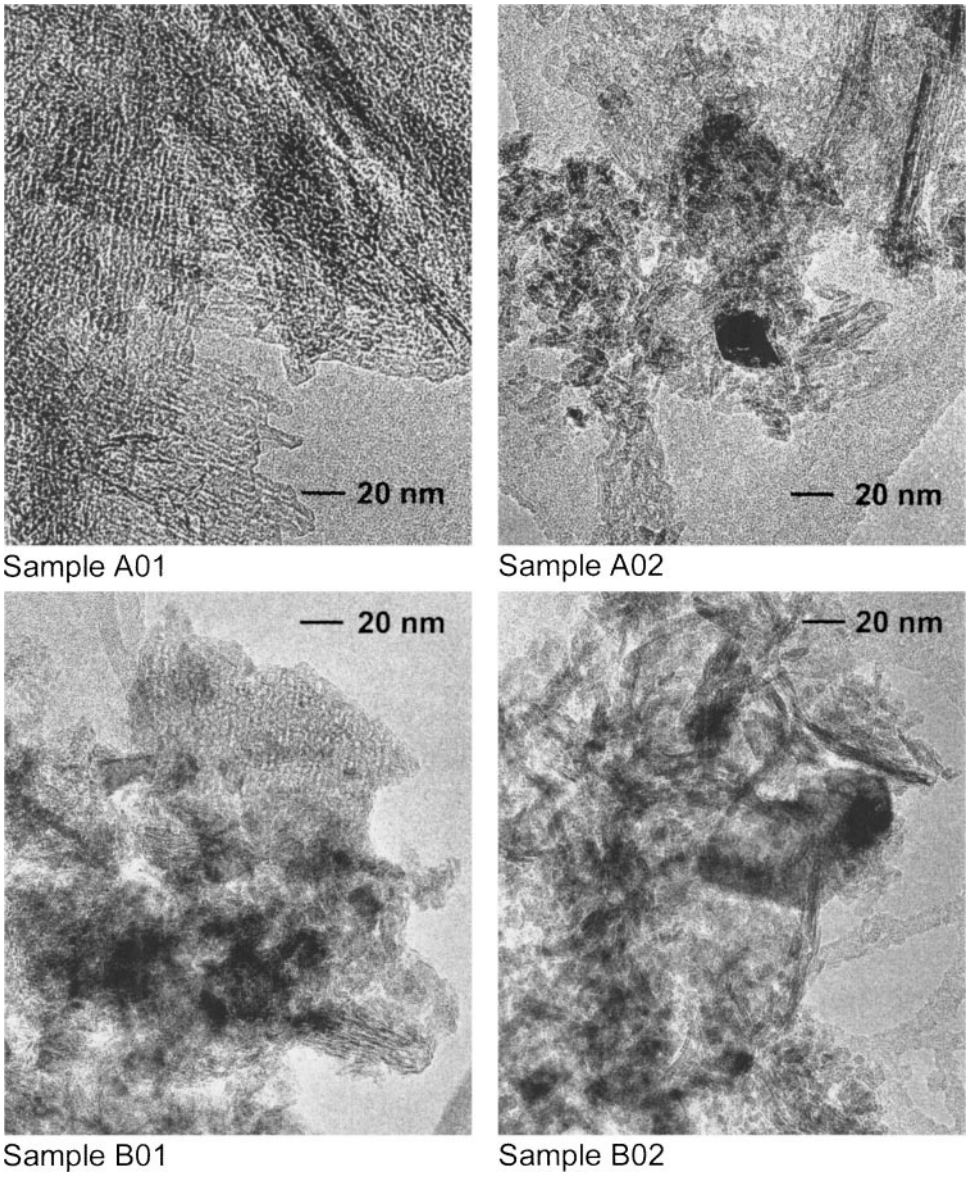

FIG. 3. TEM images of materials after calcination: 37 wt% Ni/Al_2O_3 (top) and 56 wt% Ni/Al_2O_3 (bottom).

Whereas the reducibility is changed by treating in moist air, the metal particle size is hardly influenced for all samples tested.

In the TPR patterns of the passivated 33 wt% Ni/Al_2O_3 samples (Fig. 11), treated at different temperatures and varying time, three bands can be distinguished. The first maximum is reached at temperatures between 180 and 260°C, corresponding to the reduction of the passivation layer of oxygen. Sample C2 shows a second maximum at 300°C, reflecting the reduction of bulk nickel oxide. The reduction of nickel aluminate species is found at temperatures between 500 and 900°C.

For the passivated 54 wt% Ni/Al_2O_3 samples, two bands may be distinguished in the TPR patterns (Fig. 11). The reduction of the passivation layer of oxygen takes place at temperatures between 180 and 260°C. The reduction of nickel aluminate is found at temperatures between 350 and 850°C. With increasing pretreatment temperature and time, more nickel aluminate is formed.

4. DISCUSSION

Following the coprecipitation steps, the resulting hydrotalcite was subjected to various calcination procedures. In particular, we have investigated the use of a stagnant gas phase, thereby soaking the product in water vapour or acidic gases liberated during calcination, and the use of efficient stripping, thereby avoiding a long contact time of mentioned gases and the solid product of calcination.

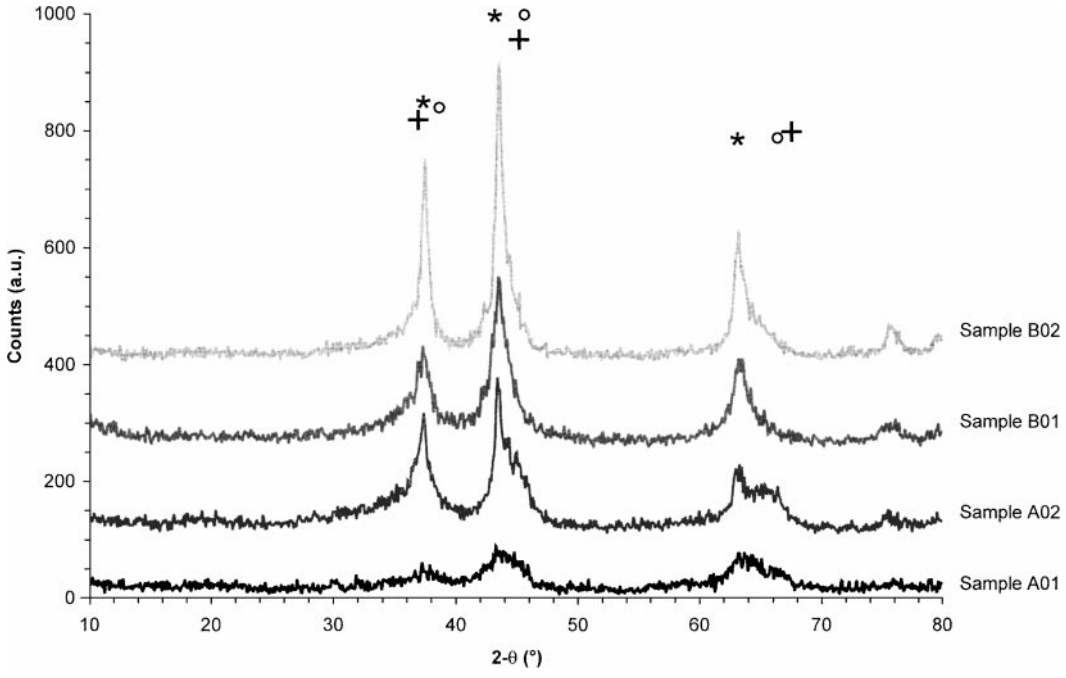

FIG. 4. XRD patterns of the calcined Ni/Al_2O_3 samples: (∗) reflections of nickel oxide; (○) reflections of Al_2O_3; (+) reflections of $NiAl_2O_4$.

The alumina-supported nickel materials in this study were derived from a hydrotalcite prepared by coprecipitation of nickel and aluminum nitrates using sodium hydroxide as a precipitating agent. Impregnation or homogeneous deposition can also be used to prepare precursors for alumina-supported nickel materials. However, it is known that coprecipitation is more suited to synthesise supported materials with high metal loadings.

Water is already introduced into the hydrotalcite structure in the coprecipitation step. Upon heating the

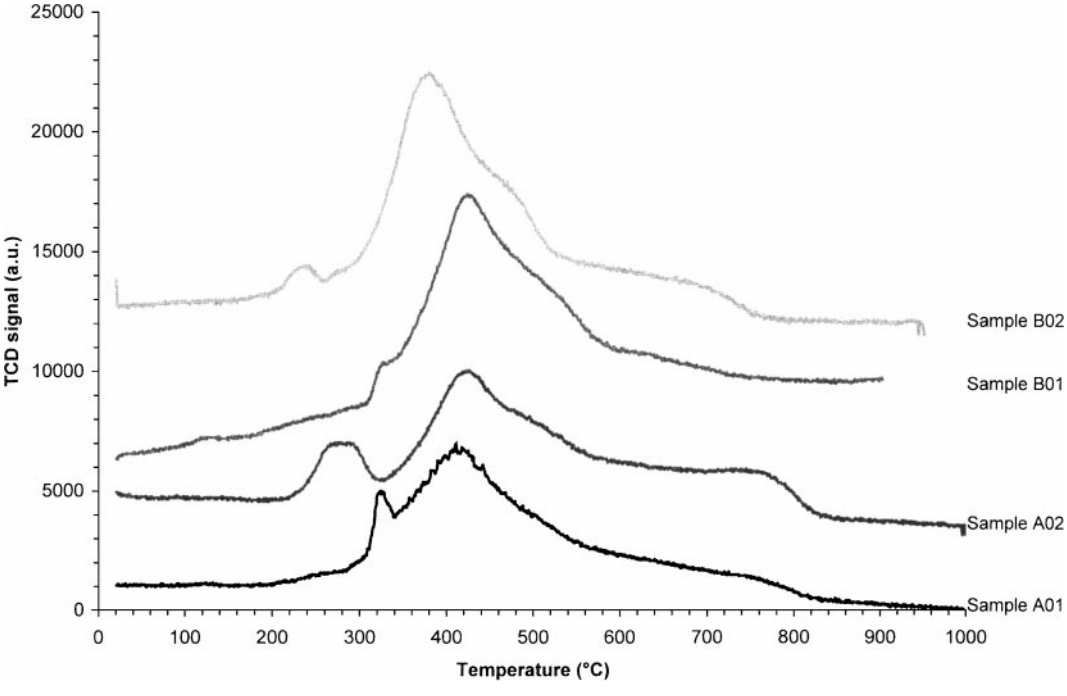

FIG. 5. TPR patterns of the calcined Ni/Al_2O_3 samples.

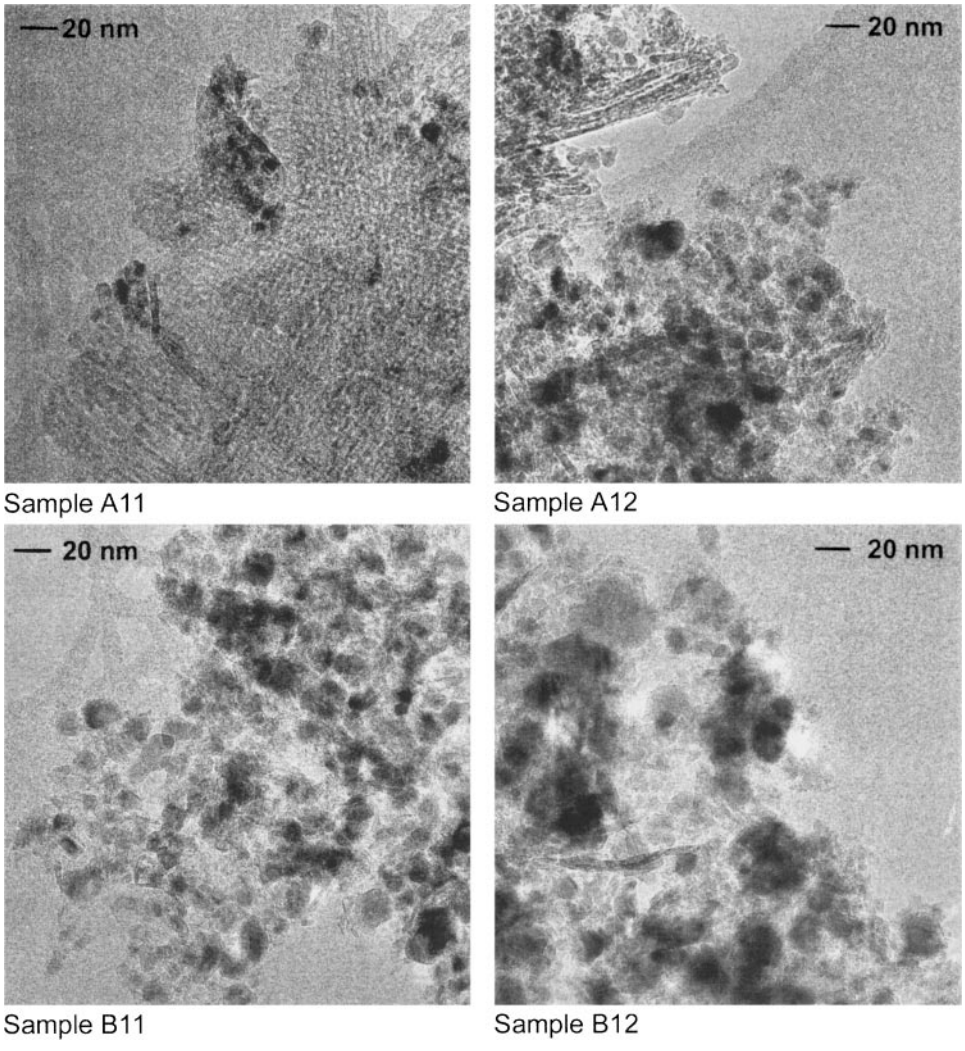

FIG. 6. TEM images of materials after passivation: 37 wt% Ni/Al_2O_3 (top) and 56 wt% Ni/Al_2O_3 (bottom).

hydrotalcite in the calcination step, the hydroxyl groups will condensate to form water.

Nitrate-based nickel and aluminum salts were used in the synthesis of the hydrotalcite material. Some nitrates still present in the hydrotalcite after thorough washing lead to the formation of acidic gases upon heating the hydrotalcite. The amount of acidic gases liberated during the calcination step might be reduced by the choice of other nickel and aluminum salts for the coprecipitation step, performing the coprecipitation at higher pH, or using a different precipitating agent. However, other authors have shown that using sodium carbonate as a precipitating agent instead of sodium hydroxide leads to the uptake of more water in the hydrotalcite (6). Due to hydrogen bonding to the carbonate ions, this water is difficult to remove.

From XRD analysis it was observed that, besides the hydrotalcite, a boehmite aluminum hydroxide phase precipitates for $x_{Ni} = 0.40$. This latter phase probably contains some nickel.

During calcination both a nickel oxide rich phase and an aluminum oxide rich phase are formed. The diffusion of nickel to the aluminum oxide rich phase and/or the diffusion of aluminum to the nickel oxide rich phase in the presence of water vapour and acidic gases was observed in TPR. Therefore, nickel becomes more surrounded by aluminum, thereby rendering reduction of nickel more difficult. The loss in the degree of reduction, as evidenced by chemisorption, is largest in the series of Ni/Al_2O_3 samples with the highest nickel metal loading.

The diffusion of nickel and/or aluminum from one phase to the other probably depends on the nickel loading. The driving force of the diffusion of nickel and/or aluminum is likely to be a concentration gradient between the nickel oxide rich phase and the aluminum oxide rich phase.

Using a combination of TEM and XRD, we could demonstrate that the nickel oxide particles supported on alumina may show a significant degree of sintering when calcination takes places under stagnant conditions. Poels *et al.* (42)

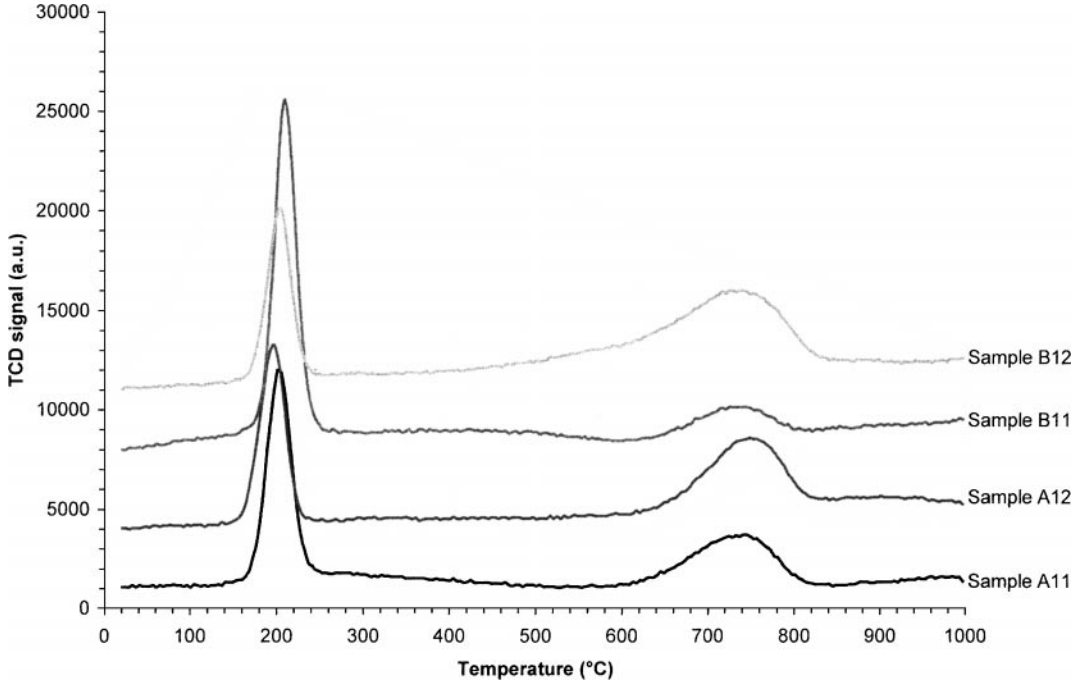

FIG. 7. TPR patterns of the passivated Ni/Al_2O_3 samples.

already demonstrated that at elevated temperatures nickel metal particles may sinter due to the presence of water. When nitrate is used as a precursor salt, this is true as well for NO_x vapours formed during calcination.

A nickel aluminate type phase at the alumina interface with the nickel oxide particle hinders the reduction of the particle (14). The nickel oxide particles in low-loaded samples are more decorated or supported by a nickel aluminate type phase, making reduction of the sample more difficult. In the case of smaller NiO particles, this interface is relatively more abundant. As a function of the Ni loading, this interface would be expected to show a maximum: for

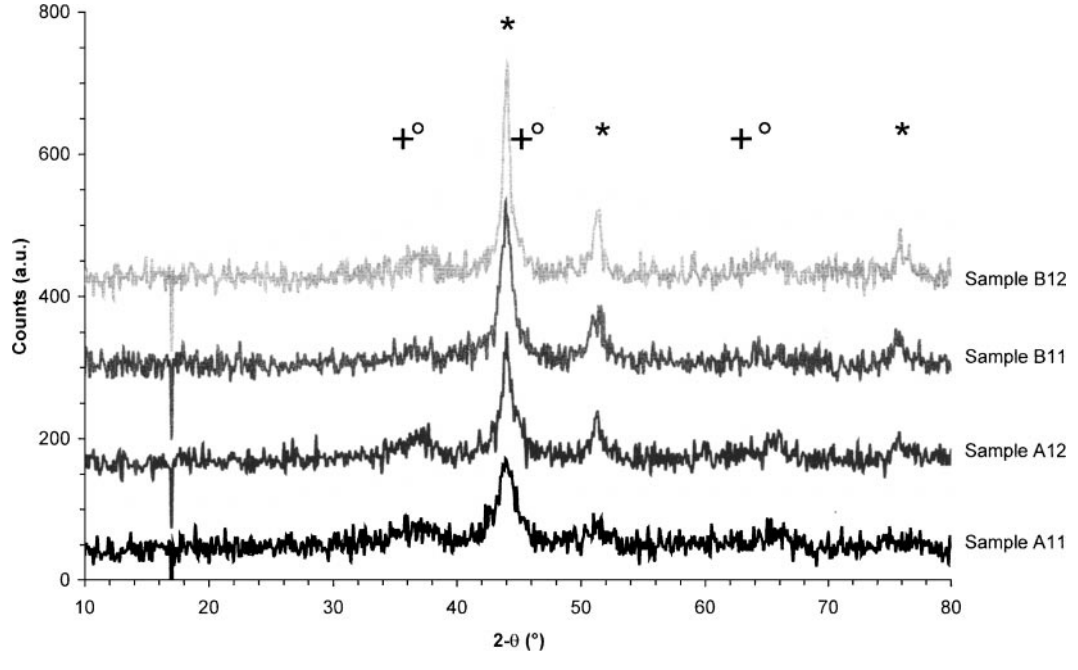

FIG. 8. XRD patterns of the passivated Ni/Al_2O_3 samples: (∗) reflections of nickel metal (Ni^0); (○) reflections of Al_2O_3; (+) reflections of $NiAl_2O_4$.

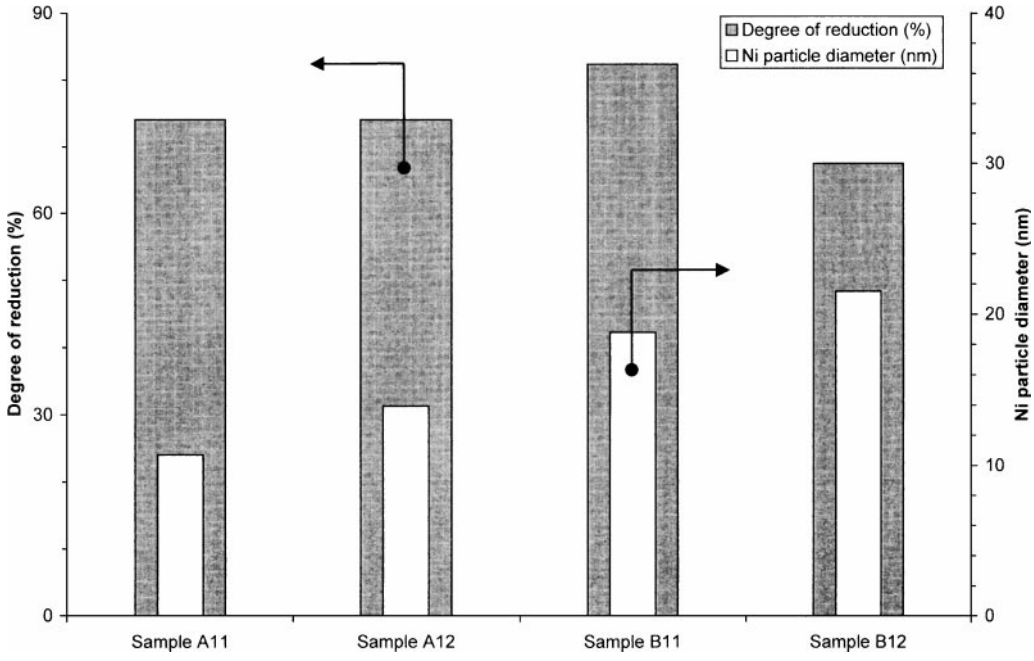

FIG. 9. Nickel particle diameter (nm) and degree of reduction (%) of Ni/Al_2O_3 samples after passivation determined by H_2 chemisorption (at room temperature) and reaction with O_2 (at 400°C), respectively.

low-loaded samples, the interface would be small, whereas the same would be true for very high loadings. Ni/Al_2O_3 samples with $x_{Ni} = 0.4$ have a comparable degree of reduction. For the samples with a higher nickel content of $x_{Ni} = 0.6$, a decrease in degree of reduction was observed after calcination under stagnant conditions. This could indeed be attributed to the comparatively small interface between the oxide and the aluminate. The nickel–aluminum compounds formed during this diffusion process are difficult to reduce. Nickel in these compounds is not reduced

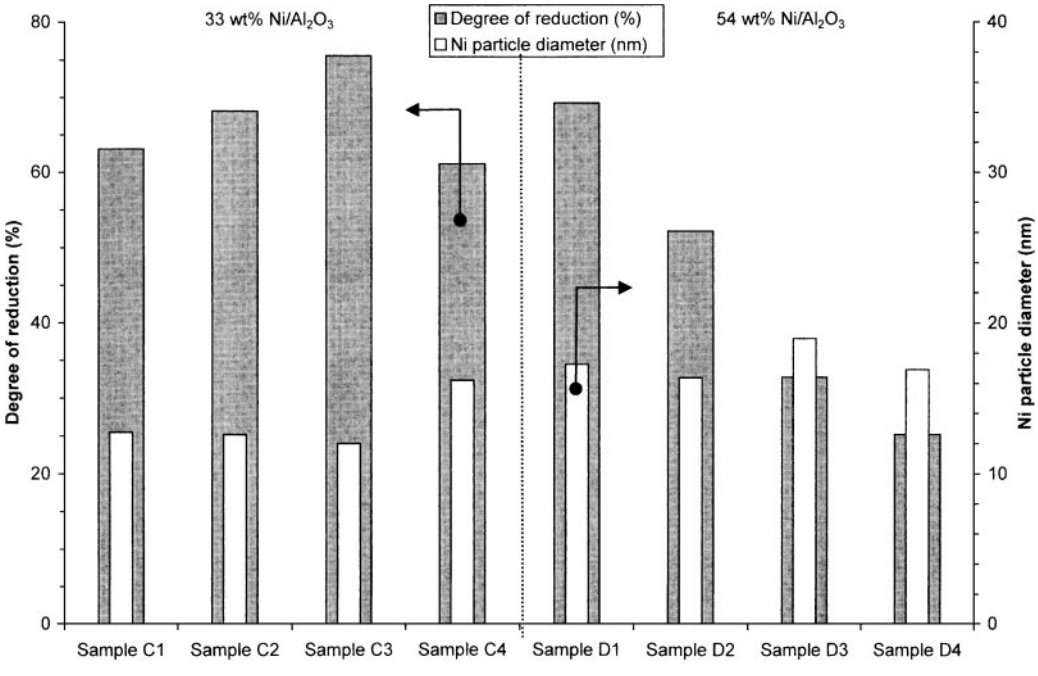

FIG. 10. Degree of reduction (%) and nickel particle diameter (nm) of Ni/Al_2O_3 samples treated at different temperatures and varying time in moist air: 33 wt% Ni/Al_2O_3 (left); 54 wt% Ni/Al_2O_3 (right).

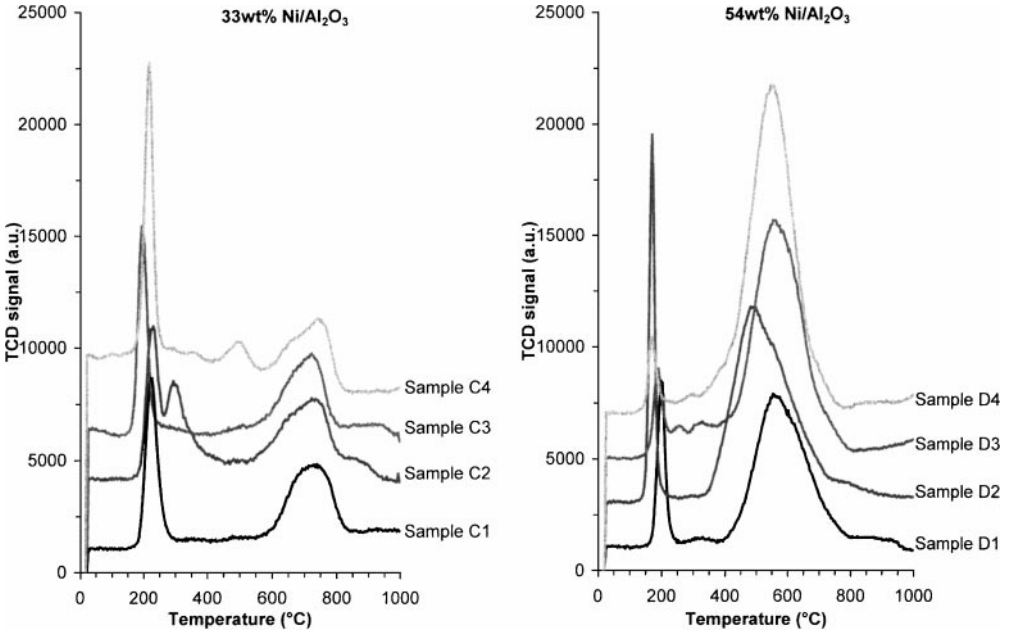

FIG. 11. TPR patterns of passivated Ni/Al_2O_3 samples calcined at different temperatures and varying time in moist air: 33 wt% Ni/Al_2O_3 (left); 54 wt% Ni/Al_2O_3 (right).

at 550°C, even when reduction is carried out for as long as 24 h.

After calcination, the nickel oxide particles are stabilised against sintering by a nickel aluminate type phase at the surface of the particles. The treatment of the calcined low-loaded Ni/Al_2O_3 sample in moist air initially led to an increase in the degree of reduction. Due to the presence of water vapour, nickel becomes less surrounded by aluminum. It is suggested that this is perhaps due to a recrystallisation of the aluminum oxide rich phase, whereby nickel diffuses out of the aluminum oxide phase.

Although the nickel crystallites are less surrounded by alumina, no increase in the diameter of the metallic nickel particles is observed. This indicates that the nickel particles are stable toward sintering under the reduction method employed.

A prolonged treatment of the calcined material in moist air at 550°C, however, promotes the formation of nickel aluminate (43).

For the calcined high-loaded sample, the same treatment in moist air leads to a steady decrease in the degree of reduction. Due to the higher Ni/Al ratio, migration of nickel into the aluminum oxide rich phase and/or migration of aluminum into the nickel oxide rich phase is promoted. The nickel becomes more surrounded by aluminum, rendering reduction more difficult.

5. CONCLUSIONS

In the present work, the influence of the calcination conditions on the eventual structure of alumina-supported nickel particles was studied. During each subsequent step of the preparation procedure, the structure of the material was analysed.

Precursor materials for Ni/Al_2O_3 samples were prepared using coprecipitation. After coprecipitation, a hydrotalcite is formed. As was also observed by other authors, a separate phase also precipitates for a Ni/Al molar ratio $x_{Ni} \leq 0.5$. This phase is boehmite.

Water is already introduced into the hydrotalcite structure in the coprecipitation step. Upon heating the hydrotalcite in the calcination step, the hydroxyl groups will condensate to form water. Some nitrates still present in the hydrotalcite after thorough washing will lead to the formation of acidic gases upon heating the hydrotalcite. The amount of acidic gases liberated during the calcination step might be reduced by the choice of other nickel and aluminum salts for the coprecipitation step, performing the coprecipitation at higher pH, or using a different precipitating agent.

Upon calcination of the precursor material, particles are formed containing more nickel than the surrounding material. The surrounding material consists of a nickel-containing aluminum oxide phase and a nickel aluminate spinel-type phase. Calcination in the presence of water vapour and acidic gases leads to sintering of the nickel oxide particles. A high Ni/Al ratio promotes the interdiffusion of nickel into the aluminum oxide rich phase and/or the diffusion of aluminum into the nickel oxide rich phase. This eventually leads to a material with larger nickel metal particles and a lower degree of reduction under more severe calcination conditions.

Further treatment of calcined samples in moist air mainly affects the degree of reduction. After calcination, the nickel oxide particles are stabilised against sintering by a nickel aluminate type phase at the surface of the particles. For samples with $x_{Ni} = 0.4$, the degree of reduction increases with treatment temperature. This is thought to arise from migration of nickel out of the aluminum oxide rich phase, either by recrystallisation of the aluminum oxide rich phase or by the extraction of nickel from this aluminum oxide phase. The degree of reduction for $x_{Ni} = 0.7$ decreases with increasing treatment temperature.

The two competing mechanisms occurring are recrystallisation of the alumina phase (including phase segregation) and mixed oxide formation by ionic diffusion. At low nickel loading, it seems recrystallisation is predominant, perhaps due to the largely amorphous nature of the precursors and the existence of a separate aluminum-containing phase at $x_{Ni} = 0.4$. At $x_{Ni} = 0.6$ (B samples) or 0.7, stable hydrotalcite compound formation is feasible and the development of both larger crystallites (not unambiguously) and lower degree of reduction bears evidence to the occurrence of the two processes described above, ion diffusion being the predominant one in this case.

ACKNOWLEDGMENTS

We thank J. Majeski and J. W. Elgersma for preparing and characterising the samples calcined in moist air and ICP-AES experiments, W. Molleman for performing the XRD experiments, and Dr. P. J. Kooyman of the National Centre for High Resolution Electron Microscopy, Delft University of Technology, for performing electron microscopy investigations. The Graduate School for Process Technology OSPT is gratefully acknowledged for financial support.

REFERENCES

1. Thomas, C. L., "Catalytic Processes and Proven Catalysts." Academic Press, London, 1970.
2. Feitknecht, W., *Helv. Chim. Acta* **25**, 555 (1942).
3. Feitknecht, W., and Gerber, M., *Helv. Chim. Acta* **25**, 131 (1942).
4. Reichle, W. T., *J. Catal.* **94**, 547 (1985).
5. Clause, O., Gazzano, M., Trifiro, F., Vaccari, A., and Zatorski, L., *Appl. Catal.* **73**, 217 (1991).
6. Kruissink, E. C., van Reijen, L. L., and Ross, J. R. H., *J. Chem. Soc., Faraday Trans. 1* **77**, 649 (1981).
7. Lansink Rotgerink, H. G. J., Bosch, H., van Ommen, J. G., and Ross, J. R. H., *Appl. Catal.* **27**, 41 (1986).
8. Alzamora, L. E., Ross, J. R. H., Kruissink, E. C., and van Reijen, L. L., *J. Chem. Soc., Faraday Trans. I* **77**, 665 (1981).
9. Titulaer, M. K., Jansen, J. B. H., and Geus, J. W., *Clays Clay Miner.* **42**, 249 (1994).
10. Doesburg, E. B. M., Hakvoort, G., Schaper, H., and van Reijen, L. L., *Appl. Catal.* **7**, 85 (1983).
11. Rouiller, C. O., and Assaf, J. M., *Chem. Eng. Sci.* **51**, 2921 (1996).
12. Rikhter, K., Ketchik, S. V., Simonova, L. G., and Borisova, M. S., *Kinet. Catal.* **16**, 1121 (1975).
13. Kis, E., Marinkovic-Neducin, R., Lomic, G., Boskovic, G., Obadovic, D. Z., Kiurski, J., and Putanov, P., *Polyhedron* **17**, 27 (1998).
14. Clause, O., Rebours, B., Merlen, E., Trifiro, F., and Vaccari, A., *J. Catal.* **133**, 231 (1992).
15. Twigg, M. V., and Richardson, J. T., *Appl. Catal. A: Gen.* **190**, 61 (2000).
16. Rebours, B., d'Espinose de la Caillerie, J. B., and Clause, O., *J. Am. Chem. Soc.* **116**, 1707 (1994).
17. Lamber, R., and Schulz-Ekloff, G., *J. Catal.* **146**, 601 (1994).
18. Ross, J. R. H., and Steel, M. C. F., *J. Chem. Soc., Faraday Trans.* **69**, 10 (1973).
19. Ross, J. R. H., Steel, M. C. F., and Zeini-Isfahani, A., *J. Catal.* **52**, 280 (1978).
20. Zielinski, J., *J. Mol. Catal.* **83**, 197 (1993).
21. Zielinski, J., *Appl. Catal. A: Gen.* **94**, 107 (1993).
22. Zielinski, J., *Catal. Lett.* **12**, 389 (1992).
23. Kruissink, E. C., Pelt, H. L., Ross, J. R. H., and van Reijen, L. L., *Appl. Catal.* **1**, 23 (1981).
24. Borisova, M. S., Dzis'ko, V. A., and Simonova, L. G., *Kinet. Catal.* **15**, 425 (1974).
25. de Korte, P. H. M., Doesburg, E. B. M., de Winter, C. P. J., and van Reijen, L. L., *Solid State Ionics* **16**, 73 (1985).
26. Noskova, S. P., Borisova, M. S., Dzis'ko, V. A., Khisamieva, S. G., and Alabuzhev, Y. A., *Kinet. Catal.* **15**, 527 (1974).
27. Simonova, L. G., Dzis'ko, V. A., Borisova, M. S., Karakchiev, L. G., and Olen'ko, I. P., *Kinet. Catal.* **14**, 1380 (1973).
28. Bish, D. L., and Brindley, G. W., *Am. Mineral.* **62**, 458 (1977).
29. Scheffer, B., Molhoek, P., and Moulijn, J. A., *Appl. Catal.* **46**, 11 (1989).
30. Kloprogge, J. T., and Frost, R. L., *Appl. Catal. A: Gen.* **184**, 61 (1999).
31. Bartholomew, C. H., and Farrauto, R. J., *J. Catal.* **45**, 41 (1976).
32. Zielinski, J., *J. Catal.* **76**, 157 (1982).
33. Zielinski, J., *J. Chem. Soc., Faraday Trans.* **93**, 3577 (1997).
34. Richardson, J. T., Lei, M., Turk, B., Forster, K., and Twigg, M. V., *Appl. Catal. A: Gen.* **110**, 217 (1994).
35. Richardson, J. T., Turk, B., and Twigg, M. V., *Appl. Catal. A: Gen.* **148**, 97 (1996).
36. Rynkowski, J. M., Paryjczak, T., and Lenik, M., *Appl. Catal. A: Gen.* **106**, 73 (1993).
37. Gil, A., Diaz, A., Gandia, L. M., and Montes, M., *Appl. Catal.* **109**, 167 (1994).
38. Wanke, S. E., and Flynn, P. C., *Catal. Rev.* **12**, 93 (1975).
39. Bartholomew, C. H., and Pannell, R. B., *J. Catal.* **65**, 390 (1980).
40. Lansink Rotgerink, H. G. J., van Ommen, J. G., and Ross, J. R. H., *in* "Preparation of Catalysts IV" (B. Delmon, P. Grange, P. A. Jacobs, and G. Poncelet, Eds.), p. 795. Elsevier, Amsterdam, 1987.
41. Cesteros, Y., Salagre, P., Medina, F., and Sueiras, J. E., *Appl. Catal. B: Environ.* **25**, 213 (2000).
42. Poels, E. K., Dekker, J. G., and van Leeuwen, W. A., *in* "Preparation of Catalysts V" (G. Poncelet, P. A. Jacobs, P. Grange, and B. Delmon, Eds.), p. 205. Elsevier, Amsterdam, 1991.
43. Bolt, P. H., Habraken, F. H. P. M., and Geus, J. W., *Catal. Lett.* **39**, 233 (1996).